

# Automatic Stent Segmentation in IOCT images using Combined Feature Extraction Techniques and Mathematical Morphology

Matheus Cardoso Moraes, Diego Armando Cardona Cardenas, Sérgio Shiguemi Furuie

School of Engineering, University of São Paulo, Brazil

## Abstract

*Atherosclerosis causes millions of deaths and billions in expenses worldwide. Intravascular Optical Coherence Tomography (IOCT) is an intravascular imaging modality, used in coronary visualization and neo-intima post stent re-stenosis investigation. Segmentation is important for the re-obstruction quantification, improving the overall procedures. As IOCT is relatively new, few fully automatic stent segmentation works can be found in the literature. Since IOCT provides hundreds of images, non-automatic segmentation procedures may be an arduous task. Consequently, we present a fully automatic stent segmentation methodology, based on a combination of contrast stretching; wavelet decompositions as Feature Extraction; and morphological reconstruction used as post-processing so as to select and improve the previous obtained information. The evaluation was performed by segmenting 160 images from pig coronaries, containing a variety of stent disposition; hence, the outcomes were compared with their corresponding gold standards. The final results led to: True Positive (%) =  $93.35 \pm 6.49$ , and False Positive (%) =  $8.05 \pm 11.6$ . The outcome provided accurate values; in addition, it is a complete automatic approach.*

## 1. Introduction

Atherosclerosis is the cause of millions of deaths and billions of dollars in costs around the world [1]. Intravascular Optical Coherence Tomography (IOCT) is a Medical Imaging Modality based on infrared-light and catheter, important for coronary analysis. Among applications, it allows investigation of neo-intima post stent re-stenosis. However, segmentation is important for the re-obstruction quantification; hence, accelerating interventions, stent investigations and improving diagnostics and therapies [2, 3, 4]. Because IOCT produces hundreds of images during a pullback, manual or even semi-automatic segmentation process may become a stressful and time-consuming task. The literature presents good segmentation methods, for intravascular modalities, IOCT and IVUS, using

statistical features, gradients, energy minimization process, Wavelets, Otsu, and Fuzzy [2 - 7], yet few are dedicated to automatic stent segmentation, which may be the major bottleneck. Therefore we adapted the methods presented at [4 - 6] to create a fully automatic stent segmentation approach, based on a combination of Feature Extraction operations followed by a Morphological Reconstruction used as post-processing.

## 2. Methodology

This approach aims to present the methodology, segmenting a set of IOCT images and assesses the accuracy, comparing the obtained outcomes to their corresponding gold standards made manually by experts. A total of 160 IOCT images were obtained from pigs in the Heart Institute of the University of São Paulo, Brazil (InCor), where the ethics and study protocol were approved by the competent committee.

The methodology is divided into three steps. The **Preprocessing** enhance important images properties (Figure 1). The **Feature Extraction** extracts specific information by Wavelet and binary threshold. Finally, the **Binary Morphological Image Reconstruction** selects some of the relevant information extracted previously to generate the stent contour, concluding the segmentation (Figures 3, 4 and 5).

*Preprocessing* – The purpose of this block is to enhance stent information, increasing the distinction between stent and tissue; hence, facilitating feature extraction. Firstly, the alignment marks (Figure 1(a)) must be removed, because they may be misinterpreted as stent during feature extraction; hence, as their positions and intensity level are known, a local 3x3 median filter is carried out. After the alignment marks filtering, a lumen segmentation procedure is performed using [5, 6], the pixels of the lumen object received the value correspondent to the maximum average level of the  $I_{Original}$ ; for instance, mean plus 3\*standard deviation of  $I_{Original}$ . The lumen object, with new pixel's values, is added to the image generating  $I_{Clean}$  (Figure 1(b)); hence, a domain conversion, taking the image to the polar domain is performed (Figure 1(c)). The domain, lumen object with the computed values are important for feature

extraction and morphological operations [4 - 6]. Finally, in order to isolate and enhance the most relevant information, finishing the preprocessed image (Figure 1(g)) a histogram stretching procedure takes place. Therefore, firstly the most important information from  $I_{Polar}$  is selected  $I_{Selected}$  (Figures 1(d)), it is generated by an AND operation between  $I_{Polar}$  and  $I_{PolarBin}$ , where  $I_{PolarBin}$  is a binary version of the  $I_{Polar}$  using Otsu threshold [8]. This operation removes low level intensities from  $I_{Polar}$ , since the stent level has intensity above average. Next, a histogram stretching procedure stretches the histogram of  $I_{Selected}$ ,  $H_{Selected}$  (Figures 1(e)), generating  $H_{Stretched}$  (Figures 1(f)). The correspondent  $H_{Stretched}$  image,  $I_{Stretched}$  is filtered by an SRAD filter, resulting in  $I_{PreProc}$  (Figures 1 (g)). The stretch procedure increases the discrimination between stent and rest of image, while speckle features is attenuated with SRAD.

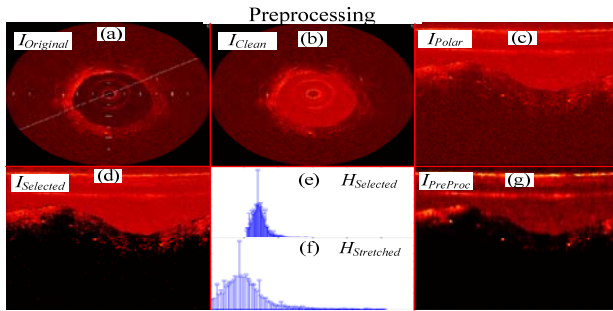


Figure 1. Preprocessing. (a) Original image. (b) Image after lumen segmentation and local marks cleaned ( $I_{Cleaned}$ ). (c) The cleaned image ( $I_{Cleaned}$ ) converted to the polar domain, Polar image ( $I_{Polar}$ ). (d) Image with information selected by its binary version with otsu threshold The cleaned image ( $I_{Selected}$ ). (e) and (f) Histogram of ( $I_{Selected}$ ) and its stretched version, respectively. (g) Final Pre-processed image ( $I_{PreProc}$ ) obtained by the  $H_{Stretched}$  followed by SRAD.

**Feature Extraction** – The Feature Extraction combines Wavelet and gray level threshold to extract useful information from the  $I_{PreProc}$ . Therefore, nine levels of the Discrete Wavelet Packet Frame (DWPF) decomposition, using Daubechies 1 ( $db1$ ) was performed (Figure 2) [4-6], generating the Coefficients of approximation Matrices,  $cAn$  and Coefficients of details Matrices,  $cD^x n$ , where  $n$  are the level and  $x$  the direction of detail coefficient. The DWPF was chosen because it does not subsample with decompositions, important for the morphological operation. The wavelet mother and number of decomposition were chosen based on what information brought by coefficients could be combined for stent extraction.

In order to combine information during the *Binary Morphological Image Reconstruction*, the resultant wavelet coefficients are binarized using as threshold level 99% of the maximum corresponding coefficient histogram; hence, the regarding binary coefficients are:

$$\begin{aligned} cAn_{bin} &= \{1 | i \geq 0.99 \times \max(hist(cAn))\} \\ cD^x n_{bin} &= \{1 | i \geq 0.99 \times \max(hist(cD^x n))\} \end{aligned} \quad (1)$$

where,  $i$  and  $hist$  are the pixel intensity level and histogram of regarding coefficient, and  $cAn_{bin}$  and  $cD^x n_{bin}$  are the binary version of the corresponding coefficients. The threshold level of 99% is because stent and important tissue information are as high as the top 1% wavelet coefficient values. The  $cD^h 5_{bin}$ , binary lumen,  $cA5_{bin}$  and  $cA9_{bin}$ , (Figures 3 (a), (b), (e) and (f) and (Figures 4 (a), (b), (e) and (f)) binary versions of their respective wavelet coefficients were chosen as a root of information so as to extract stent information during the next section.

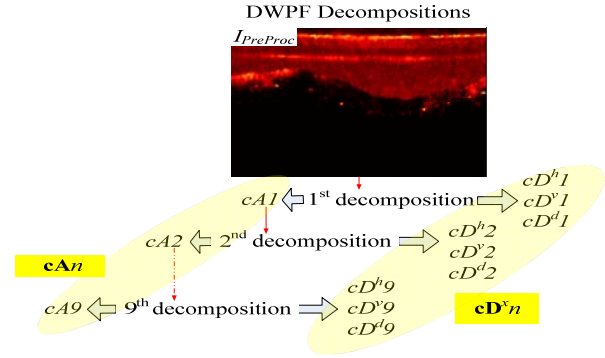


Figure 2. Illustration of the 9 Discrete Wavelet Packet Frame Decompositions (DWPF).  $cAn$  Coefficients of approximation Matrices.  $cD^x n$  Coefficients of details Matrices.

**Binary Morphological Image Reconstruction** – A set of mathematical morphology operations [4-6] was combined aiming the reconstruction of the stent contour in Cartesian coordinates  $I_{StentContourCartesian}$  (Figure 5(f)).

The operations are divided in 2 major blocks, the first is the **Morphological Stent Extraction and Selection** and the second is the **Cartesian Image Reconstruction**. The first block is composed by two strategies to obtain the stent information. The second uses the obtained stent information  $Inf_{Stent}$  (Figure 5(a)) to build the  $I_{StentContourCartesian}$  (Figure 5(f)).

**Morphological Stent Extraction and Selection** - Since the infrared is very sensible to the thickness of the neointimal tissue, producing different image features depending on the distance between lumen and stents, two parallel procedures are used to obtain stent information in both situations. The procedures extract information close and far from the lumen (Figures 3(d), and (h)), next a decision for which one will be the source of stent information is made. Specifically in the original image (Figure 1(a)), there is no large neointimal tissue, that is why  $Inf_{StentClose}$  (Figures 3(d)) provided more information than  $Inf_{StentFar}$  (Figures 3(h)); hence,  $Inf_{StentClose}$  would be the chosen source in this situation. An opposite example, where there is a big neointimal tissue can be seen at

Figure 4; hence,  $Inf_{StentClose}$  (Figures 4(d)) provided less information than  $Inf_{StentFar}$  (Figures 4(h)), where in this case the last would be the source. The procedure to extract  $Inf_{StentClose}$  and  $Inf_{StentFar}$  is explained below:

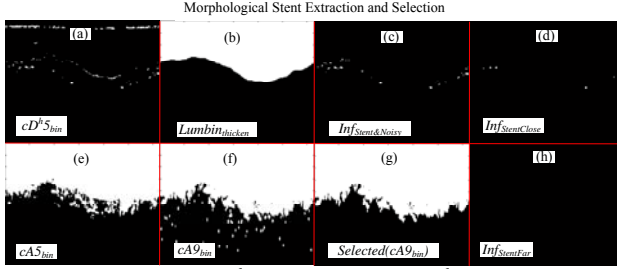


Figure 3. (a)  $cD^h5_{bin}$ , the binary  $cD^h5$  (b)  $Lumenbin_{thicken}$ , the binary lumen thick of 5 pixel. (c)  $Inf_{Stent\&Noisy}$ , Stent and remaining Noisy information. (d) Stent Information close to the lumen (e) and (f)  $cA5_{bin}$  and  $cA9_{bin}$ , the binary versions of  $cA5$  and  $cA9$  (g)  $Selected(cA9_{bin})$  the  $cA9$  after a binary area selection by region growing. (h) Stent Information far from the lumen.

#### Extraction of the Stent Information close to the lumen

- This procedure uses two data,  $cD^h5_{bin}$  and  $Lumenbin_{thicken}$ , (Figures 3(a) and (b)) produced by Feature Extraction and the segmented lumen, respectively, to generate stent information merged with noisy,  $Inf_{Stent\&Noisy}$ , (Figure 3(c)), obtained by:

$$Inf_{Stent\&Noisy} = cD^h5_{bin} \vee Lumenbin_{thicken}, \quad (2)$$

where,  $\vee$  is an OR operation,  $cD^h5_{bin}$  and  $Lumenbin_{thicken}$  are the binary versions of the  $cD^h5$  and polar lumen object thickened by 5 pixels. The information,  $cD^h5_{bin}$  was chosen because it is the best among binary coefficients to extract stent information close to the lumen, merged with some tissue, and by performing an OR between  $cD^h5_{bin}$  and the negation of the  $Lumenbin_{thicken}$ ,  $\overline{Lumenbin_{thicken}}$ , the lumen border information contained in  $cD^h5_{bin}$  are mostly removed. Finally, to remove the remaining noisy in  $Inf_{Stent\&Noisy}$  an opening procedure is carried out, generating  $Inf_{StentClose}$  (Figure 3(d)):

$$Inf_{StentClose} = Inf_{Stent\&Noisy} \circ S_{circ(3)}, \quad (3)$$

where,  $\circ$  is an opening procedure, and  $S_{circ(3)}$  is a circular structure with diameter 3 pixels [4-6]. This size assures noisy removal with low stent information damage.

**Extraction of the Stent Information far from the lumen** – Here,  $cA5_{bin}$  and  $cA9_{bin}$ , (Figures 4(e) and (f)), obtained during Feature Extraction, are used as source of information. First a binary area selection at  $cA9_{bin}$ , separates the lumen and neointimal region from the rest, generating the  $Selected(cA9_{bin})$  (Figures 4(g)). Once we have this information, the stents far from the lumen are extracted by:

$$Inf_{StentFar} = cA5_{bin} \vee \overline{Selected(cA9_{bin})}, \quad (4)$$

where,  $\vee$  is an OR operation,  $cA5_{bin}$  is the binary versions of  $cA5$  and  $\overline{Selected(cA9_{bin})}$  is the negation of

$Selected(cA9_{bin})$ , where after the OR between  $cD^h5_{bin}$  and  $Selected(cA9_{bin})$ , only the stent is maintained. Therefore stent information far from the lumen, usually because big neointimal tissue, are extracted; as it was not the case at Figure 3, we demonstrate with Figure 4.

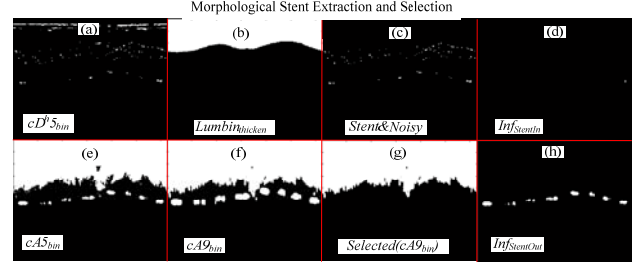


Figure 4. The Same procedure presented in Figure 3, yet using other image, in which the stent information is extracted by  $Inf_{StentOut}$

**Stent Information selection** – The criteria to decide which stent information should be used, (Figures 3(d) or (h)) or in the other case (Figures 4(d) or (h)), relies on comparing which one produced more information, i.e. which has more white pixels:

$$Inf_{Stent} = \begin{cases} Inf_{StentClose} & \text{if } Inf_{StentClose} \geq Inf_{StentFar} \\ Inf_{StentFar} & \text{otherwise} \end{cases}, \quad (5)$$

In Figure 3, it can be observed that the only information extracted here was  $Inf_{StentClose}$  (Figure 3(d)); therefore, it will be used as the source of information  $Inf_{Stent}$  during next procedure (Figure 5(a)).

**Cartesian Image Reconstruction** – Once the source of information  $Inf_{Stent}$  is decided (Figure 5(a)), the height of the stent is taken  $Inf_{StentFilled}$  and transformed in signal  $s(Inf_{StentFilled})$  to be interpolated  $s(Interpolated)$ , using Piecewise cubic Hermite interpolation [4-6] (Figure 5(b), (c) and (d)). Consequently, a polar and Cartesian Image of the interpolated signal could be computed (Figure 5(e) and (f)), in which the contour of the Cartesian image is extracted and placed on the original Image, finalizing the segmentation (Figure 6).

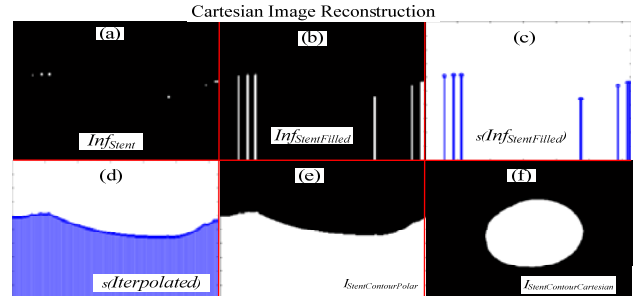


Figure 5. (a)  $Inf_{Stent}$ , the binary stent information (b)  $Inf_{StentFilled}$ , the stent information filled downwards. (c) and (d) signals representing the column heights of the  $Inf_{StentFilled}$ , and its interpolation, respectively. (e) and (f) The corresponding stent contour in the Polar and Cartesian coordinates.

### 3. Results

The evaluation was carried out by processing 160 IOCT images from Pig's coronaries. The images were acquired by an IOCT (St. Jude/LightLab Optical Coherence Tomography – St. Jude Medical, Inc., Westford, Massachusetts, USA), with pullback of 0.5mm/s, and 20f/s in the Heart Institute of the University of São Paulo database, Brazil (InCor). A desktop with an Intel Core 2 Duo 2.53 GHz, 4 GB of RAM, Windows Vista 32 bits and MATLAB (2009a) were used to perform the computation and evaluation. The average of stent segmentation time was (35.22±2.78)s. The segmentation accuracy is corroborated by comparing the segmented images to Gold Standards made by experts, the parameters of accuracy, True Positive (*TP*), False Positive (*FP*) and False Negative (*FN*), were computed (Table 1). As it can be seen, the *TP* is over 93% while the *FP* and *FN* are around 8% and 6%, respectively. The results are in line with previous study [2].

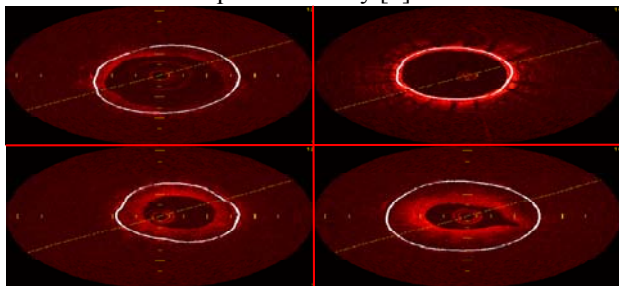


Figure 6. Segmentation Outcome.

Table 1. Assessment of accuracy.

T P(%)	F P(%)	F N(%)
93.35±6.49	8.05±11.6	6.65±6.49

### 4. Discussion and conclusion

In spite of improvements, a complete IOCT segmentation method with good accuracy, practicability and cost, for lumen and stent, is still being pursued. Consequently, a new and alternative methodology, using wavelet, Otsu and morphological operation, effectively applied in former studies [4-6], was modified and applied in this approach, providing a new solution for stent segmentation.

A set of images with a variety of features was used to test and corroborate the method (Table 1) (Figure 6). As it could be seen in Table 1, there is a high agreement between the methods and manual segmentation. In addition, the results are similar to the proposed by [2]. Despite the fact that comparing outcomes from different studies might not bring deep conclusion, as dataset are different, this comparison may be a good indicator of usefulness.

In conclusion, the accuracy, the low computational cost, and practicability for being fully automatic make this approach an alternative tool for stent segmentation in IOCT images helping investigators in quantitative neointimal investigation. Indeed, the accuracy and computational cost still have space for improvements. Therefore, future works will focus on better parameters choices and code optimization to improve accuracy and computational efficiency.

### Acknowledgements

São Paulo Research Foundation – Brazil (**FAPESP** – Process Number: 2012/15721-2), National Council of Scientific and Technological Development – Brazil (**CNPq**), Heart Institute of University of São Paulo – Brazil (**InCor**), Biomedical Engineering Laboratory of the State University of São Paulo – Brazil (**LEB-USP**).

### References

- [1] Wayne R, Katherine F, Gary F, Karen F, Alan G, Kurt G, et al. Heart disease and stroke statistics–2007 update: a report from the American Heart Association Statistics Committee and Stroke Statistics Subcommittee. *Circulation* 2007;115(5):e69–171.
- [2] Tsantis S, Kagadis G, Katsanos K, Karnabatidis D, Bourantas G, Nikiforidis G. Automatic vessel lumen segmentation and stent strut detection in intravascular optical coherence tomography. *Medical Physics* 2012; 39: 503-13.
- [3] Nico B, Kenji S, Jurgen L, Sebastiaan de W, Evelyn R. Automated three-dimensional detection of tomography images. *Computing in Cardiology*, 2011;38: 221-224.
- [4] Matheus CM, Sérgio SF. Automatic coronary wall segmentation in intravascular ultrasound images using binary morphological reconstruction. *Ultrasound in Medicine & Biology* 2011;37:1486-99.
- [5] Matheus CM, Diego ACC, Sérgio SF. Automatic IOCT lumen segmentation using wavelet and mathematical morphology. *Computing in Cardiology* 2012;39:545-48.
- [6] Matheus CM, Diego ACC, Sérgio SF. Automatic lumen segmentation in IVOCT images using binary morphological reconstruction. *BioMedical Engineering OnLine* 2013;12(78): in press.
- [7] Jayaram KU, Punan KS. Fuzzy connectedness and image segmentation. *Proceedings of the IEEE* 2003; 91(10): 1649-1669.
- [8] Nobuyuki O. A threshold selection method from gray-level histograms. *IEEE Trans Syst Man Cybern C Appl Rev* 1979;9(1):62–6.

Address for correspondence.

Matheus Cardoso Moraes

Laboratório de Engenharia Biomédica – Departamento de Telecomunicações e Controle - Escola Politécnica da USP - Av. Prof. Luciano Gualberto, Travessa 3, 158 - sala D2-06, CEP 05508-970 São Paulo - SP – Brazil  
matheuscardosomg@hotmail.com